mater.scichina.com link.springer.com

Published online 26 May 2023 | https://doi.org/10.1007/s40843-023-2449-8
Sci China Mater 2023, 66(8): 3046–3053

High-voltage electrolyte design for a Ni-rich layered oxide cathode for lithium-ion batteries

Jun Hu[†], Fangyuan Cheng[†], Chun Fang[*] and Jiantao Han[*]

ABSTRACT **$LiNi_{0.8}Co_{0.1}Mn_{0.1}O_2$ (NCM811) is one of the most promising cathode materials in high-energy-density Li-ion batteries (LIBs) because of its high capacity and low cost. However, it still suffers from irreversible capacity fading at high cut-off voltages. This is mainly because high voltage accelerates the hydrolysis reaction of lithium hexafluorophosphate with trace water to generate byproducts such as highly corrosive hydrogen fluoride (HF) resulting in an unstable cathode–electrolyte interface and continuous irreversible phase transitions. Here, we modify a conventional electrolyte by adding the dual additives of tetrabutyl titanate (TBT) and lithium difluoroxalate borate (LiDFOB) to form a stable Ti-, B-, and F-rich interfacial layer to eliminate the unfavorable cathode-electrolyte side reactions and suppress deleterious phase transitions. Additionally, TBT can stabilize the electrolyte by removing H_2O/HF. With the synergistic effect of the dual additives, the cycling stability of NCM811 at high voltages is enhanced considerably. The Li|NCM811 cell with dual additives exhibits a high capacity retention rate of 86% after 200 cycles at 1 C and a high cut-off voltage of 4.5 V. This strategy provides a reference for designing high-voltage electrolytes for LIBs.**

Keywords: lithium-ion batteries, $LiNi_{0.8}Co_{0.1}Mn_{0.1}O_2$, electrolyte, high voltage, additives

INTRODUCTION

With the rapid development of electric vehicles, intelligent equipment, electronic communication, and other industries, the market demand for high-energy lithium-ion batteries (LIBs) is increasing [1–3]. The cathode material is a crucial part of LIBs and greatly impacts battery performance. To date, dozens of cathode materials have been developed, among which Ni-rich layered oxide $LiNi_{0.8}Co_{0.1}Mn_{0.1}O_2$ (NCM811) is one of the most popular cathode materials because of its high energy density and low cost [4–6].

For NCM811 cathode materials, as the charging voltage increases from 4.3 to 4.5 V, the specific discharge capacity increases from 195 to 210 mA h g^{-1}, which is very beneficial for improving the cruising range of electric vehicles [7]. However, increasing the charging cut-off voltage will also bring more serious side reactions at the cathode–electrolyte interface and phase transitions [8,9]. Particularly, the hydrolysis of $LiPF_6$-containing electrolytes is caused by the combination and decomposition of PF_6^- with trace water in the electrolyte. High voltage catalyzes this hydrolysis reaction, mainly because of the decrease in the oxidative stability of the structure after the combination of PF_6^- and water, and the energy barrier of the decomposition reaction decreases, eventually intensifying the hydrolysis reaction. The hydrogen fluoride (HF) present in the highly corrosive hydrolysate will attack the cathode–electrolyte interface film and active materials, eventually leading to unstable interfacial phases and irreversible phase transitions from the surface. Therefore, determining how to inhibit the combination of PF_6^- and water in the electrolyte and form a stable cathode–electrolyte interphase is the key to improve the cycling stability of high-voltage LIBs. To solve the above problems and improve the cycle stability of LIBs with NCM811 under high voltages, many improvement strategies have been proposed [10–12]. As previously reported, the interphase layer between the surface of the cathode and the electrolyte is designed to improve the electrochemical performance by nanocoating, which serves to regulate the interfacial chemistry, prevent the dissolution of transition metals (TMs), and suppress the interfacial side reactions [13–16]. Xu's group [17] added an appropriate amount of lithium difluorophosphate to a common commercial electrolyte to extend the cycling life of the $Li|LiNi_{0.76}Mn_{0.14}Co_{0.10}O_2$ cell at high voltages. The improvement mechanism is that lithium difluorophosphate can form a strong interphase on the cathode surface. Tris(trimethylsilyl) phosphite [18] was used to remove HF from the electrolyte to improve the electrochemical performance of high-voltage LIBs. Improving the interface or removing HF from the electrolyte can improve the cycling stability of LIBs at high voltages to a certain extent, but few studies consider both approaches.

Only forming the interface film and neglecting the HF steadily released from the electrolyte deposition lead to the continuous decomposition of the electrolyte under high voltages [19]. Conversely, when removing H_2O/HF without using a stable interface film, the cathode is in direct contact with the electrolyte. The high voltage causes the electrophilic alkyl carbonate to react with the nucleophilic cathodic oxygen [20]. Both of the above situations reduce the long-cycle stability of the battery. In this study, we modified the conventional electrolyte by adding dual additives of tetrabutyl titanate (TBT) and lithium difluoroxalate borate (LiDFOB). LiDFOB and TBT can form a stable Ti-, F-, and B-rich cathode–electrolyte interphase to prevent side

State Key Laboratory of Material Processing and Die & Mould Technology, School of Materials Science and Engineering, Huazhong University of Science and Technology, Wuhan 430074, China

[†] These authors contributed equally to this work.

[*] Corresponding authors (emails: fangchun@hust.edu.cn (Chun F); jthan@hust.edu.cn (Han J))

 © Science China Press 2023

reactions between the cathode and electrolyte. TBT can remove H_2O/HF to stabilize the electrolyte and reduce the HF erosion of active materials. TBT and LiDFOB act synergistically to eliminate the unfavorable cathode–electrolyte interfacial reactions and suppress the irreversible phase transitions. The cycling stability of NCM811 at high voltages is enhanced considerably. The NCM811|Li cell with dual additives exhibits a high capacity retention rate of 86% after 200 cycles at 1 C and a high cut-off voltage of 4.5 V. In contrast, after 200 cycles, the cell with the baseline electrolyte only retains 39.1% of its original capacity.

EXPERIMENTAL SECTION

Preparation of electrodes and electrolytes

NCM811 (from Ronbay Technology) was selected as the cathode material, and lithium metal (thickness: 200 μm, from China Energy Lithium Co., Ltd.) was the anode material. NCM811, super P, and polyvinylidene fluoride were mixed in a ratio of 7:2:1 in *N*-methyl-2-pyrrolidone (NMP) to configure the cathode slurry. The cathode slurry was coated on an aluminum foil and dried under vacuum at 100°C for 8 h. The active material loading of the cathode was 4 mg cm^{-2}. The electrolyte composed of 1 mol L^{-1} $LiPF_6$ in ethylene carbonate/diethyl carbonate (EC/DEC, 1:1 by volume) was named the baseline. The electrolyte obtained by adding 1% TBT or 0.1 mol L^{-1} LiDFOB as an additive to the baseline was named TBT and LiDFOB, respectively, and that obtained by adding TBT and LiDFOB as dual additives was named TBT-LiDFOB. Finally, 2025-type cells were assembled in an argon glove box. The amount of electrolyte employed was 90 μL, and Celgard 2500 was used as the separator.

Electrochemical performance testing

The electrochemical performance of the coin-type cells was evaluated with a Neware battery test system. For cycling performance measurements, the assembled cell was rested for 8 h before being activated at 0.2 C and then used for a long-cycle performance test. Electrochemical impedance spectroscopy (EIS) was applied at 0.1–100,000 Hz. Cyclic voltammetry (CV) curves were measured using stainless-steel|Li cells at 0.15 mV s^{-1}.

Chemical analysis and material characterization

Nuclear magnetic resonance (NMR) spectra were recorded on a Bruker AV400 spectrometer to analyze the reaction products of TBT and H_2O/HF. The morphology of the cycled electrodes was measured with scanning electron microscopy (SEM, JSM 7600F). X-ray diffraction (XRD, X-Pert Pro MRD) was measured at 2θ = 10°−80° using Cu Kα radiation. X-ray photoelectron spectroscopy (XPS, ESCALAB 250Xi) was used to detect the element valence on the surface of the samples. Transmission electron microscopy (TEM, JEM-2100) was performed to characterize the morphology differences of cathode electrolyte interphase (CEI). The TM dissolution was measured using an inductively coupled plasma optical emission spectrometer (ICP-OES, Prodigy Plus).

RESULTS AND DISCUSSION

Trace amounts of HF in the electrolyte will accelerate electrolyte degradation under a high voltage [8]. The HF in the electrolyte generally comes from the hydrolysis of lithium hexafluorophosphate, which produces byproducts such as PF_5, and PF_5 will further catalyze the decomposition or polymerization of the solvent and cause the electrolyte to become discolored and turbid. HF is highly corrosive and corrodes the cathode–electrolyte interface film and active material, leading to battery failure [9]. Therefore, the elimination of H_2O/HF is also crucial for the electrolyte. TBT is known for its ability to scavenge water and HF. Here, the color change of electrolytes and ^{19}F NMR spectroscopy were used to evaluate the ability of different electrolytes to remove H_2O/HF. Fig. 1a, b show the initial state of the baseline and TBT electrolytes, respectively, and the color change with 1000 ppm H_2O after 10 days of storage is shown in Fig. 1c, d. The baseline electrolyte showed obvious discoloration and turbidity, while the TBT electrolyte changed from an original yellow color (TBT color) to transparent, indicating that TBT has been hydrolyzed. The color change of different electrolytes without 1000 ppm H_2O after 10 days of storage is shown in Fig. S1. The baseline electrolyte remained basically unchanged, while the TBT electrolyte changed to a near-transparent state, indicating that the solvent inevitably contains trace water; however, the storage time is not long enough to change the color of the baseline electrolyte, and TBT has been hydrolyzed. The ^{19}F NMR spectra in Fig. 1e show that the baseline sample exhibits two peaks. The peak at ~75 ppm is related to the PF_6^- anion from the $LiPF_6$ salt, while the peak at ~158 ppm is the characteristic signal of HF [21,22]. These F-containing species were produced by the decomposition of $LiPF_6$ in the presence of a trace amount of H_2O, and HF tends to undergo adverse reactions with active materials. In contrast, almost no HF peak was observed in the ^{19}F NMR spectrum of the TBT-containing sample, indicating that TBT can remove H_2O/HF in the electrolyte and increase the stability of the electrolyte.

Fig. 1f, g show the CV curves of electrolytes with and without additives on stainless-steel|Li cells. Fig. 1f shows that the initial oxidation potential of the first CV curve is lower in TBT-LiDFOB than in the baseline electrolyte, which should be due to the preferential oxidation and decomposition of additives. However, no obvious oxidation peak is observed in TBT-LiDFOB during the second CV cycle (Fig. 1g), indicating that the electrolyte has been isolated from the cathode by an additive-derived interface. Conversely, a sharp oxidation peak is observed for the baseline electrolyte in the second cycle, revealing that this electrolyte is continuously decomposing. The comparison in Fig. 1g demonstrates that once a stable interface layer is formed through preferential oxidation and decomposition of the additives in the first cycle, the decomposition of the electrolyte will be inhibited in the subsequent cycles to maintain sufficient stability during cycling.

To explore the superiority of TBT and LiDFOB as electrolyte additives, the electrochemical performance of the NCM811|Li cells was tested, as shown in Fig. 2 and Figs S2–S6. Figs S2 and S3 show the electrochemical performance of the NCM811|Li cells with different contents of TBT and LiDFOB. Compared with cells with 0.5% TBT and 2% TBT, cells with 1% TBT as an additive have higher capacity retention. Furthermore, the optimal addition of LiDFOB is 0.1 mol L^{-1}. Fig. 2a displays the specific discharge capacity of the cells with baseline and TBT electrolytes at 2.7–4.3 V. After 200 cycles, the capacity retention rate of the cell with TBT is 83.2%, while the baseline cell remains at 66.4% of the original capacity. Fig. 2b displays the specific discharge capacity of both cells at 2.7–4.5 V. After 200 cycles, the capacity retention rate of the cell with TBT is 75.1%, while the baseline cell remains at only 39.1% of the original capacity.

© Science China Press 2023

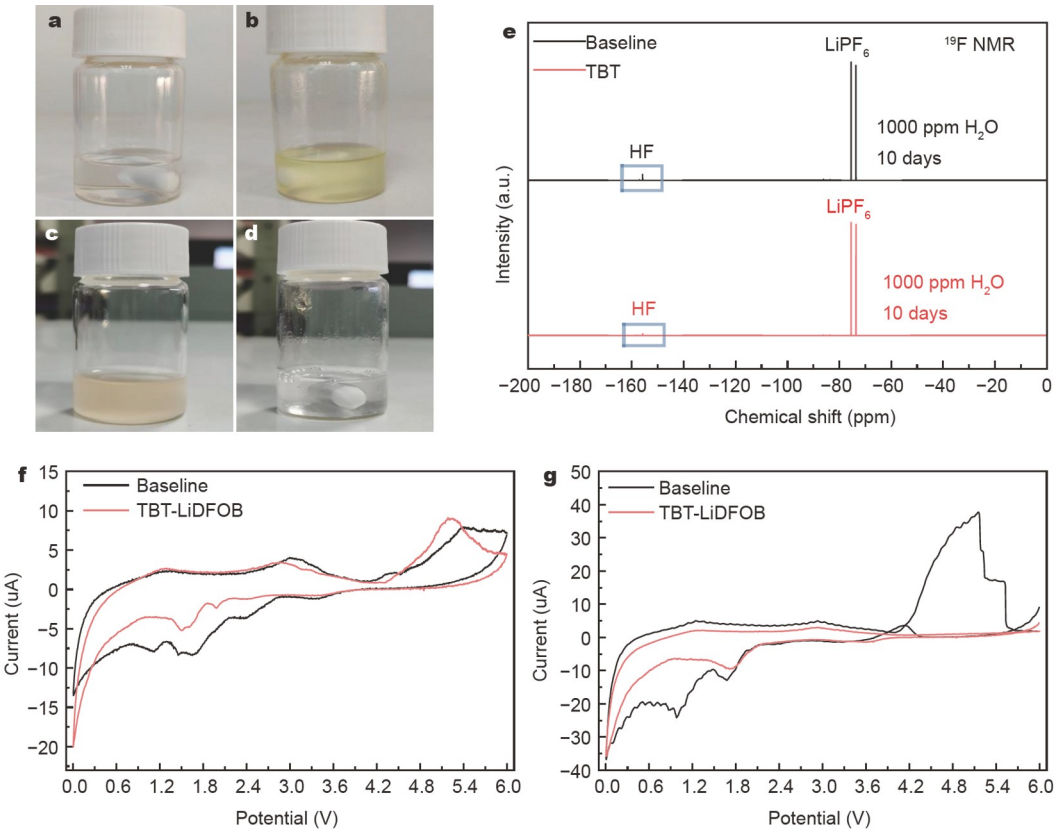

Figure 1 Color change of different electrolytes: (a) baseline, (b) TBT, (c) baseline with 1000 ppm H_2O after 10 days of storage, and (d) TBT with 1000 ppm H_2O after 10 days of storage; (e) ^{19}F NMR spectra of the different electrolytes with 1000 ppm H_2O after storage at 25°C for 10 days; oxidative potentials of the baseline and TBT-LiDFOB electrolytes at 0.15 mV s^{-1}: (f) the first and (g) the second CV curves.

Fig. 2c shows the specific discharge capacity of the NCM811|Li cells with the baseline electrolyte and the TBT-LiDFOB electrolyte at 4.5 V, and Fig. S4 shows the corresponding first charge–discharge curves. At a high cut-off voltage of 4.5 V, the cell with dual additives shows a much higher initial coulombic efficiency than the baseline cell, and it exhibits a high capacity retention of 86.0% over 200 cycles. The cell with LiDFOB obtained a capacity of 70.3% at 2.7–4.5 V over 200 cycles, which is much lower than the cells with TBT-LiDFOB (Fig. S5). Thus, the cell with dual additives has better high-voltage cycling stability than the baseline cell and the cell with individual additives. Fig. S6 shows the rate performance of the NCM811|Li cells with different electrolytes. At 0.2–2 C, the cells cycling in different electrolytes essentially have identical discharge capacities, but when the rate is higher than 5 C, the discharge capacity of the TBT-LiDFOB cell is considerably higher than that of the baseline. Fig. 2d, e further show the charge–discharge curves for the 10th–200th cycles of the cells cycled at a 1-C rate in different electrolytes with and without dual additives. In the 10th cycle, both cells have similar voltage profiles, with a voltage plateau near 3.8 V. After 50 cycles, the cell with the baseline electrolyte shows a substantial voltage drop and a disappearance of the plateau, implying that the crystal structure was severely distorted and the lithiation/delithiation kinetics deteriorated. However, the cell with TBT-LiDFOB still maintains a perfect voltage profile with no severe voltage drop.

XPS was used to analyze the chemical compositions of the NCM811 cathode surface after five cycles. The XPS spectra in Fig. 3 provide detailed information about the CEI composition. The C 1s spectrum (Fig. 3a, b) shows that the sample cycled in the dual-additive-modified electrolyte has an obvious COOR peak, indicating that LiDFOB is involved in cathode–electrolyte interphase formation. In the F 1s spectrum (Fig. 3c, d, i), a less substantial LiF peak is observed in the sample containing TBT and LiDFOB, indicating that the additives inhibit the decomposition of salt in the electrolyte. The higher the highest occupied molecular orbital (HOMO) energy level, the more easily the substance loses electrons. For the electrolyte, the HOMO energy level can be used to determine the oxidation order of each component during the charging process, and the component with the highest HOMO energy level undergoes oxidative decomposition first. As Fig. S7 shows, the HOMO energy level of LiDFOB is higher than that of $LiPF_6$ and the solvents of EC and DEC; thus, during the charging process, LiDFOB preferentially undergoes oxidative decomposition to stabilize the cathode–electrolyte interface. This result corresponds to the XPS result. In the O 1s spectrum (Fig. 3e, f), the electrode cycled in TBT and LiDFOB contains more C=O/C–O, suggesting that TBT contributes to CEI layer formation. The Ti 2p spectrum and B 1s spectrum (Fig. 3g, h) show that the inorganic components such as B and Ti interfacial phases are richer in the cathode–electrolyte interface of the additive-added cell than that of the baseline cell. These results imply that TBT and LiDFOB are not only involved in CEI layer formation but also may directly react with HF and inhibit LiF formation on the cathode.

Fig. 4a–d show the SEM images of the NCM811 cathode after

 © Science China Press 2023

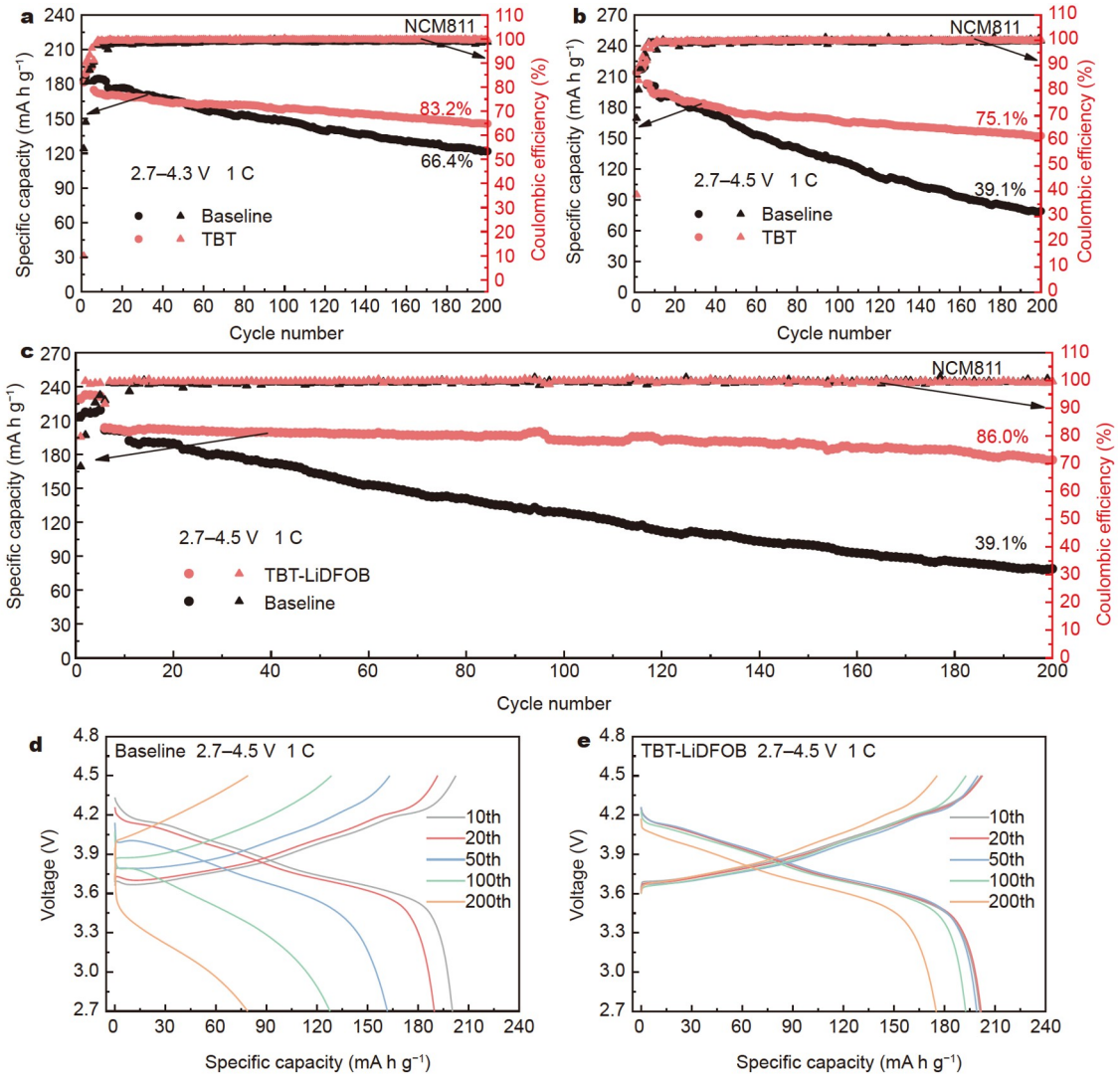

Figure 2 Electrochemical performances of NCM811|Li cells with different electrolytes: specific discharge capacity at a 1-C rate (a) from 2.7 to 4.3 V with TBT, (b) from 2.7 to 4.5 V with TBT, and (c) from 2.7 to 4.5 V with TBT-LiDFOB; (d, e) corresponding charge–discharge curves: (d) baseline and (e) TBT-LiDFOB.

200 cycles of the baseline and TBT-LiDFOB cells, respectively. The SEM images show that in all electrolytes, obvious sediments were deposited on the surface of the electrode, confirming the formation of the cathode–electrolyte interface film. The difference is that the cathode interface of the TBT-LiDFOB cell is uniformly dense and smooth, while that of the baseline cell is loose and uneven, and obvious particle fragmentation can be seen in Fig. 4b. Fig. S8 shows the SEM images of the fresh NCM811 cathode for comparison. The interface film cannot be clearly observed on the surface of NCM811 particles because of no contact with the electrolyte and no charge–discharge test. The corresponding Fourier transformed infrared (FTIR) spectrum of the cathode after 200 cycles at 2.7–4.5 V is shown in Fig. S9. Compared with the TBT-LiDFOB cathode, the baseline cathode has a spectrum with a considerably increased number of peaks in the 400–2000 cm^{-1} region (Fig. S9b), and these peaks correspond to electrolyte decomposition products such as C–O, C–H, $R_1CH{=}CHR_2$, $R_1CH{=}CH_2$, and LiF [23–25]. This result indicates that the CEI derived from dual additives is more stable, with no obvious solvent decomposition after 200 cycles at high voltage, thus slowing down the decay of the cell performance. EIS was used to study the Li-ion transport kinetics in the interfacial layer. The first semi-circle in the high-frequency region represents the interface film impedance (R_f) of the cells [26,27]. Fig. 4e, f show the impedance of NCM811|Li cells after 10 and 200 cycles in a fully discharged state to 2.7 V, and Fig. S10 shows the corresponding equivalent circuit diagram. After 10 cycles, there is an unsubstantial difference in the interfacial film impedance between the battery containing the baseline electrolyte and the battery containing the electrolyte added with TBT and LiDFOB. After 200 cycles, the bulk impedance of the electrolyte solution (R_s) and the interface film impedance R_f of the baseline cell increased considerably. In contrast, the R_s and R_f of the TBT-LiDFOB cell are much smaller than that of the baseline cell. Comparing the impedance change also revealed the greater stability of CEI derived from TBT-LiDFOB, which can suppress interfacial side reactions and reduce electrolyte consumption at high voltages.

High-resolution TEM (HR-TEM) was applied to characterize the morphology differences of CEI films derived from different

 © Science China Press 2023

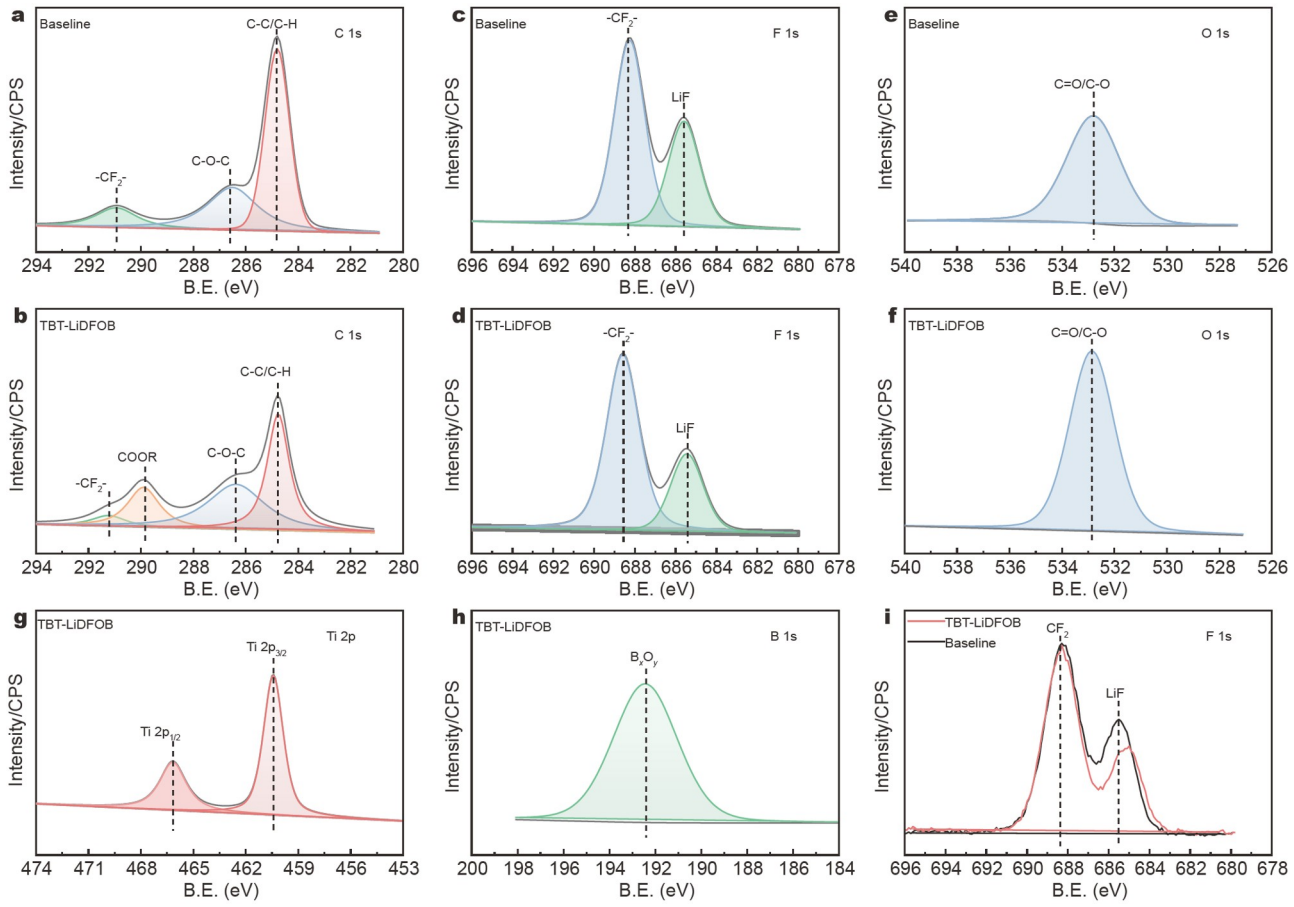

Figure 3 XPS spectra of the CEI layer of NCM811|Li cells in different electrolytes after the 5th cycle: (a, b) C 1s, (c, d, i) F 1s, (e, f) O 1s, (g) Ti 2p, and (h) B 1s; (a, c, e) baseline and (b, d, f, g, h) TBT-LiDFOB.

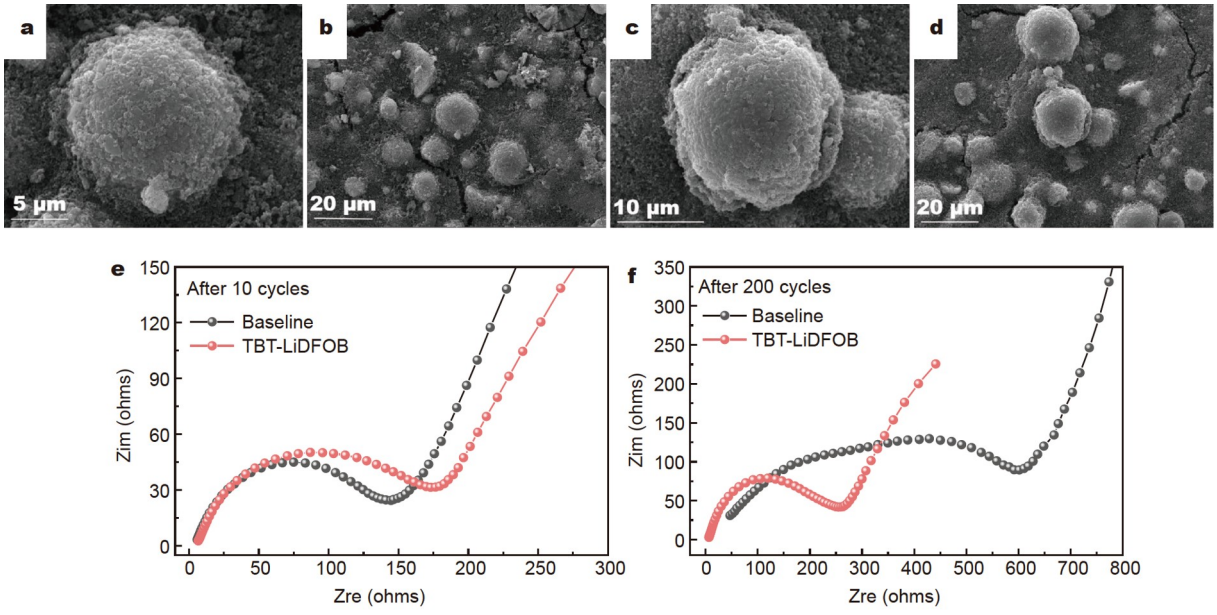

Figure 4 SEM images after 200 cycles: (a, b) baseline and (c, d) TBT-LiDFOB; (e, f) EIS of the NCM811 cathode after 10 and 200 cycles.

electrolytes after 100 cycles. As shown in Fig. 5a, a-1, the CEI generated from the baseline electrolyte is uneven and thick. In stark contrast, the CEI derived from TBT-LiDFOB is uniform and much thinner (<4 nm), as shown in Fig. 5b, b-1. To investigate the phase transformation of NCM811 during the charge–discharge process, Fig. 5c, d show the differential capa-

© Science China Press 2023

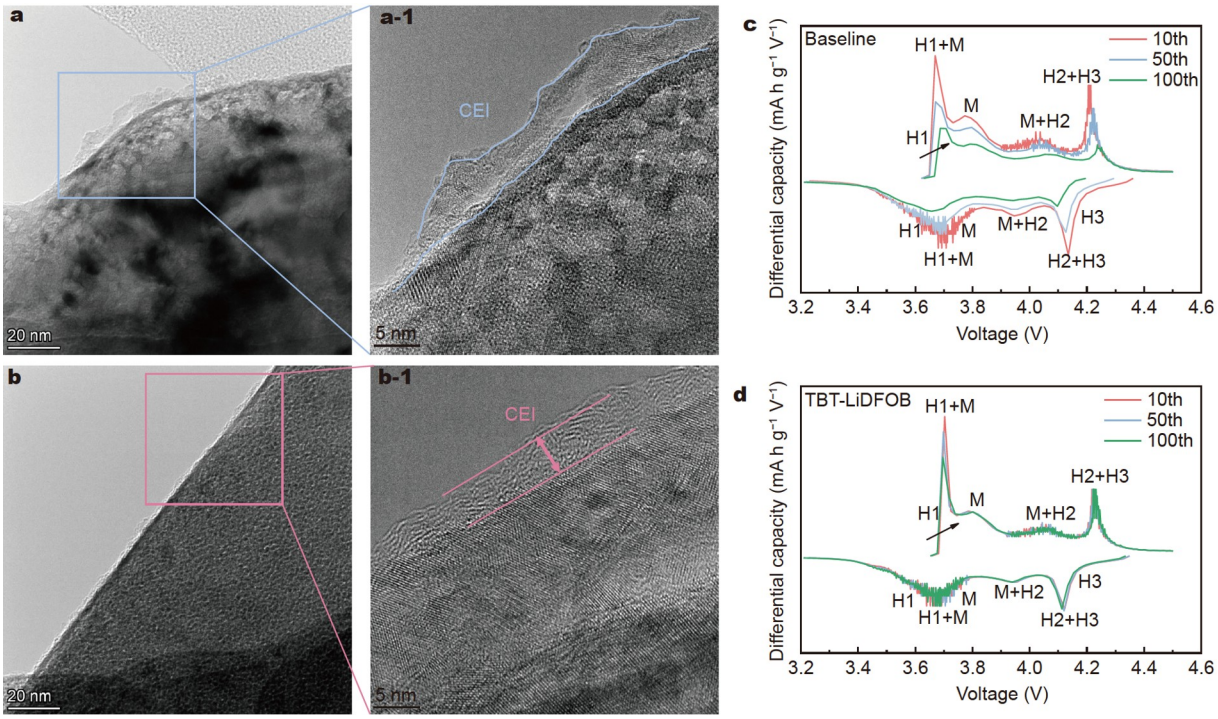

Figure 5 TEM images of the NCM811 cathode after 100 cycles at 2.7–4.5 V: (a) baseline, (b) TBT-LiDFOB; (c, d) dQ/dV (Q is the specific discharge capacity and V represents the voltage) curves for different cycles at the voltages of 2.7–4.5 V: (c) baseline, (d) TBT-LiDFOB.

city curves from the 10th to 100th cycle of the cell containing the baseline electrolyte and the cell containing the electrolyte with TBT-LiDFOB, respectively. The apparent redox peaks in the 2.7–4.5 V range correspond to the H1–M, M–H2, and H2–H3 phase transitions of the materials during Li^+ extraction and insertion, respectively [28]. The area enclosed by the curve represents the charged/discharged capacity during the phase transition. With an increasing number of cycles, the peak strength decreases considerably for the baseline cell and is well maintained for the cell with TBT-LiDFOB, which shows that the cell with the dual additives has better capacity retention than the cell with the baseline. The peak near 3.7 V represents the phase transition from the hexagonal phase (H1) to the monoclinic phase (M), and the peak near 4.0 V is associated with the phase transition from the monoclinic phase (M) to the hexagonal phase (H2). The peak at 4.2 V is related to the phase transformation from the hexagonal H2 phase to the hexagonal H3 phase. It has been reported that during the above phase transition process, the phase transition from H2 to H3 causes a release of lattice oxygens and leads to a sudden contraction of the *c*-axis lattice parameters, which causes stress accumulation inside the material particles and eventually leads to the breakage of active material particles, thus exposing more area eroded by the electrolyte, increasing the interfacial side reactions, leading to more irreversible phase transitions, and finally causing the active material to fail. The height of the H2→H3 peak of NCM811 in the baseline cell is seen to decrease substantially after 100 cycles, indicating that NCM811 undergoes an irreversible phase transition. In contrast, the height of the H2→H3 peak of the cathode in the cell containing the dual additives is well maintained, indicating a highly reversible phase transition process. Therefore, the TBT-LiDFOB dual additives can suppress the unfavorable irreversible phase transition of NCM811 by forming a stable Ti-, F-, and B-rich CEI and scavenging the highly corrosive HF. The structural changes of NCM811 after cycling in different electrolytes can also be derived from Rietveld refinement analyses of XRD patterns (Fig. S11). The diffraction peak intensity ratio of (003) to (104) crystal planes (marked as I(003)/I(104)) represents the degree of cation mixing, and a smaller I(003)/I(104) value indicates a higher degree of cation mixing and deleterious phase transformation [13,29]. According to the Rietveld refinement results, the Li/Ni cation disordered content of NCM811 is lower after cycling in TBT-LiDFOB than after cycling in the baseline electrolyte. This result indicates that the harmful phase transition due to Li/Ni mixing is suppressed by the TBT-LiDFOB-derived cathode–electrolyte interface layer. The deleterious phase transition on the surface of the NCM811 cathode may cause the dissolution of TM ions, which migrate to the Li anode surface to damage the solid–electrolyte interface. The content of TMs deposited on the Li anode after 200 cycles was tested using ICP, as shown in Fig. S12. The Li anode cycled in the baseline has severe TM deposition, particularly Ni deposition, which is as high as 0.0249 mg L^{-1}, much higher than the Li anode cycled in TBT-LiDFOB (0.0031 mg L^{-1} deposition). In addition, a substantial dissolution of Co and Mn occurs in the baseline, with dissolution amounts of 0.0043 and 0.0057 mg L^{-1}, respectively, while the dissolution amounts of Co and Mn in TBT-LiDFOB are only 0.0002 and 0.0006 mg L^{-1}, respectively. This result indicates that the Ti-, B-, and F-rich CEI formed by TBT and LiDFOB can greatly inhibit the dissolution of TMs and reduce the deposition of TM on the anode [30].

Fig. 6a, b schematize the optimization mechanism of additives. As shown in Fig. 6a, the CEI formed by the baseline electrolyte cannot prevent electrolyte decomposition from the corrosion of byproducts such as HF and, ultimately, cannot maintain a complete and uniform interface layer. Thus, side reactions at the

 © Science China Press 2023

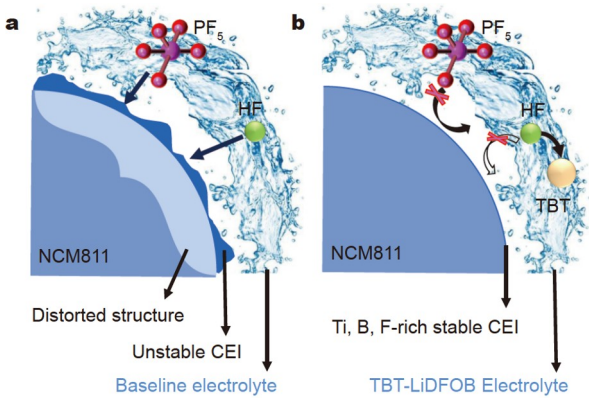

Figure 6 Schematic of the improvement mechanism with different electrolytes: (a) baseline and (b) TBT-LiDFOB.

interface and the formation of a distorted structure cause the cathode material to fail. In contrast (Fig. 6b), the TBT in the TBT-LiDFOB electrolyte can undergo a hydrolysis reaction to consume H_2O/HF in the electrolyte. In addition, the robust Ti-, F-, and B-rich CEI derived from TBT-LiDFOB can resist electrolyte erosion to ensure the stabilization of the cathode–electrolyte interface and protect the electrode surface from the erosion of PF_5 and HF. Ultimately, an irreversible deleterious phase change to a distorted structure at the interface is suppressed.

CONCLUSIONS

A high-voltage electrolyte formulation design that simultaneously improves the stability of the bulk electrolyte and cathode–electrolyte interface is proposed. In particular, under the cooperation of TBT and LiDFOB, a stable Ti-, B-, and F-rich CEI layer is formed to protect the NCM811 electrode from interfacial side reactions and phase transitions to a distorted structure. In addition, TBT stabilizes the electrolyte by removing H_2O/HF and inhibits the decomposition of the electrolyte. In the electrolyte containing TBT-LiDFOB, the NCM811|Li cell exhibits high capacity retention of 86% after 200 cycles at 1 C and a high cut-off voltage of 4.5 V. We believe that this study provides a simple electrolyte modification strategy for solving the severe capacity degradation problem of the Ni-rich NCM cathode at high voltages.

Received 7 January 2023; accepted 16 March 2023; published online 26 May 2023

1 Li M, Lu J, Chen Z, *et al.* 30 Years of lithium-ion batteries. Adv Mater, 2018, 30: 1800561
2 Liu J, Bao Z, Cui Y, *et al.* Pathways for practical high-energy long-cycling lithium metal batteries. Nat Energy, 2019, 4: 180–186
3 Choi JW, Aurbach D. Promise and reality of post-lithium-ion batteries with high energy densities. Nat Rev Mater, 2016, 1: 16013
4 Maleki Kheimeh Sari H, Li X. Controllable cathode–electrolyte interface of $Li[Ni_{0.8}Co_{0.1}Mn_{0.1}]O_2$ for lithium ion batteries: A review. Adv Energy Mater, 2019, 9: 1901597
5 Markevich E, Salitra G, Talyosef Y, *et al.* High-performance $LiNiO_2$ cathodes with practical loading cycled with Li metal anodes in fluoroethylene carbonate-based electrolyte solution. ACS Appl Energy Mater, 2018, 1: 2600–2607
6 Jung R, Metzger M, Maglia F, *et al.* Chemical *versus* electrochemical electrolyte oxidation on NMC111, NMC622, NMC811, LNMO, and conductive carbon. J Phys Chem Lett, 2017, 8: 4820–4825
7 Zhao W, Zheng J, Zou L, *et al.* High voltage operation of Ni-rich NMC cathodes enabled by stable electrode/electrolyte interphases. Adv Energy Mater, 2018, 8: 1800297
8 Liu M, Vatamanu J, Chen X, *et al.* Hydrolysis of $LiPF_6$-containing electrolyte at high voltage. ACS Energy Lett, 2021, 6: 2096–2102
9 Han JG, Kim K, Lee Y, *et al.* Scavenging materials to stabilize $LiPF_6$-containing carbonate-based electrolytes for Li-ion batteries. Adv Mater, 2019, 31: 1804822
10 Li Q, Wang Y, Wang X, *et al.* Investigations on the fundamental process of cathode electrolyte interphase formation and evolution of high-voltage cathodes. ACS Appl Mater Interfaces, 2020, 12: 2319–2326
11 Ko DS, Park JH, Yu BY, *et al.* Degradation of high-nickel-layered oxide cathodes from surface to bulk: A comprehensive structural, chemical, and electrical analysis. Adv Energy Mater, 2020, 10: 2001035
12 Cheng F, Zhang X, Qiu Y, *et al.* Tailoring electrolyte to enable high-rate and super-stable Ni-rich NCM cathode materials for Li-ion batteries. Nano Energy, 2021, 88: 106301
13 Xu GL, Liu Q, Lau KKS, *et al.* Building ultraconformal protective layers on both secondary and primary particles of layered lithium transition metal oxide cathodes. Nat Energy, 2019, 4: 484–494
14 Xu C, Märker K, Lee J, *et al.* Bulk fatigue induced by surface reconstruction in layered Ni-rich cathodes for Li-ion batteries. Nat Mater, 2021, 20: 84–92
15 Liu G, Xu N, Zou Y, *et al.* Stabilizing Ni-rich $LiNi_{0.83}Co_{0.12}Mn_{0.05}O_2$ with cyclopentyl isocyanate as a novel electrolyte additive. ACS Appl Mater Interfaces, 2021, 13: 12069–12078
16 Cherkashinin G, Eilhardt R, Nappini S, *et al.* Energy level alignment at the cobalt phosphate/electrolyte interface: Intrinsic stability *vs* interfacial chemical reactions in 5 V lithium ion batteries. ACS Appl Mater Interfaces, 2022, 14: 543–556
17 Tan S, Shadike Z, Li J, *et al.* Additive engineering for robust interphases to stabilize high-Ni layered structures at ultra-high voltage of 4.8 V. Nat Energy, 2022, 7: 484–494
18 Han YK, Yoo J, Yim T. Why is tris(trimethylsilyl) phosphite effective as an additive for high-voltage lithium-ion batteries? J Mater Chem A, 2015, 3: 10900–10909
19 Kuai D, Balbuena PB. Solvent degradation and polymerization in the Li-metal battery: Organic-phase formation in solid-electrolyte interphases. ACS Appl Mater Interfaces, 2022, 14: 2817–2824
20 Fan X, Wang C. High-voltage liquid electrolytes for Li batteries: Progress and perspectives. Chem Soc Rev, 2021, 50: 10486–10566
21 Yang X, Lin M, Zheng G, *et al.* Enabling stable high-voltage $LiCoO_2$ operation by using synergetic interfacial modification strategy. Adv Funct Mater, 2020, 30: 2004664
22 Yang X, Chen J, Zheng Q, *et al.* Mechanism of cycling degradation and strategy to stabilize a nickel-rich cathode. J Mater Chem A, 2018, 6: 16149–16163
23 Li J, Liu H, Xia J, *et al.* The impact of electrolyte additives and upper cut-off voltage on the formation of a rocksalt surface layer in $LiNi_{0.8}Mn_{0.1}Co_{0.1}O_2$ electrodes. J Electrochem Soc, 2017, 164: A655–A665
24 Zhang Y, Katayama Y, Tatara R, *et al.* Revealing electrolyte oxidation *via* carbonate dehydrogenation on Ni-based oxides in Li-ion batteries by *in situ* Fourier transform infrared spectroscopy. Energy Environ Sci, 2020, 13: 183–199
25 Ostrovskii D, Ronci F, Scrosati B, *et al.* A FTIR and Raman study of spontaneous reactions occurring at the $LiNi_yCo_{(1-y)}O_2$ electrode/non-aqueous electrolyte interface. J Power Sources, 2001, 94: 183–188
26 Xu CL, Xiang W, Wu ZG, *et al.* Constructing a protective pillaring layer by incorporating gradient Mn^{4+} to stabilize the surface/interfacial structure of $LiNi_{0.815}Co_{0.15}Al_{0.035}O_2$ cathode. ACS Appl Mater Interfaces, 2018, 10: 27821–27830
27 Shi S, Lu P, Liu Z, *et al.* Direct calculation of Li-ion transport in the solid electrolyte interphase. J Am Chem Soc, 2012, 134: 15476–15487
28 Zhang X, Qiu Y, Cheng F, *et al.* Realization of a high-voltage and high-rate nickel-rich NCM cathode material for libs by Co and Ti dual modification. ACS Appl Mater Interfaces, 2021, 13: 17707–17716
29 Li J, Li W, You Y, *et al.* Extending the service life of high-Ni layered oxides by tuning the electrode–electrolyte interphase. Adv Energy Mater, 2018, 8: 1801957

 © Science China Press 2023

30 Cheng F, Zhang X, Wei P, *et al.* Tailoring electrolyte enables high-voltage Ni-rich NCM cathode against aggressive cathode chemistries for Li-ion batteries. Sci Bull, 2022, 67: 2225–2234

Acknowledgements This work was supported by the National Natural Science Foundation of China (52172201 and 51732005). We thank the Analytical and Testing Centre and the State Key Laboratory of Materials Processing and Die & Mould Technology and the Experiment Center for Advanced Manufacturing and Technology at the School of Mechanical Science & Engineering of HUST for the material characterization. We also thank the Shiyanjia Lab (www.shiyanjia.com) for the XPS tests, the eceshi (www.eceshi.com) for the ICP tests and the SCI-GO (www.sci-go.com) for the theoretical calculation.

Author contributions Cheng F and Hu J designed and engineered the samples; Hu J performed the experiments and wrote the paper with support from Cheng F. Fang C and Han J conceived and supervised the project.

Conflict of interest The authors declare that they have no conflict of interest.

Supplementary information Supporting data are available in the online version of the paper.

Jun Hu is an undergraduate student at the School of Materials Science and Engineering, Huazhong University of Science and Technology (HUST). She majors in functional materials.

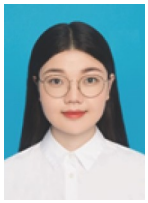

Fangyuan Cheng is a PhD candidate under the supervision of Prof. Jiantao Han at the School of Materials Science and Engineering, HUST. She received her Bachelor's degree at Hefei University of Technology in 2018. Her current research focuses on the electrolytes suitable for high-nickel ternary materials of lithium-ion batteries.

Chun Fang received her PhD degree from Fudan University in 2008. She then worked as a senior engineer at Evergreen Solar Corp. from 2009 to 2012. After that, she was an R&D manager at Empower Energy Corp. from 2012 to 2015. Currently, she is a research associate at HUST. Her research interests focus on new materials for energy storage applications.

Jiantao Han is a professor at the School of Materials Science and Engineering, HUST, China. He received his PhD degree in chemistry from Fudan University in 2007 and then worked at UT Austin (2007–2010), Los Alamos National Laboratory (2010–2012) and Pellion Tech. (2012–2014). He joined HUST as a full professor in 2016. His research interests include atomic distribution function (PDF) analysis and Li-ion batteries.

高电压高镍三元锂离子电池电解液设计

胡若[†], 程方圆[†], 方淳[*], 韩建涛[*]

摘要 $LiNi_{0.8}Co_{0.1}Mn_{0.1}O_2$ (NCM811)因具有高容量和相对低的成本, 是高能量密度锂离子电池中最有前途的正极材料之一. 然而, 在高截止电压下, 它仍然存在不可逆的容量衰减问题. 主要原因是高电压加速了六氟磷酸锂与微量水的水解反应, 产生副产物, 如高腐蚀性HF, 导致不稳定的正极-电解液界面和持续的不可逆相变. 在这里, 我们通过添加钛酸四丁酯和二氟草酸硼酸锂双重添加剂来改善传统的电解液, 以形成一个稳定的富含Ti、B和F的界面层, 从而消除不利的正极-电解液副反应并抑制有害相变. 此外, 钛酸四丁酯可以通过去除H_2O/HF来稳定电解液. 在双重添加剂的协同作用下, NCM811在高电压下的循环稳定性得到明显增强. 采用双添加剂的Li||NCM811电池在1 C和4.5 V的高截止电压下循环200次后具有86%的高容量保持率. 该方法为设计锂离子电池的高电压电解液提供了参考.

 © Science China Press 2023